AD_____

Award Number: DAMD17-00-1-0195

TITLE: Tactile Mapping of Breast Palpation for Diagnosis, Documentation and Training

PRINCIPAL INVESTIGATOR: Rujirutana A. Srikanchana

CONTRACTING ORGANIZATION: The Catholic University of America
Washington, D.C. 20064

REPORT DATE: September 2003

TYPE OF REPORT: Annual Summary

PREPARED FOR: U.S. Army Medical Research and Materiel Command
Fort Detrick, Maryland 21702-5012

REPORT DOCUMENTATION PAGE

Form Approved
OMB No. 074-0188

1. AGENCY USE ONLY (Leave blank)	2. REPORT DATE	3. REPORT TYPE AND DATES COVERED
	September 2003	Annual Summary (1 Sep 2000 - 31 Aug 2003)

4. TITLE AND SUBTITLE
Tactile Mapping of Breast Palpation for Diagnosis, Documentation and Training

5. FUNDING NUMBERS
DAMD17-00-1-0195

6. AUTHOR(S)
Rujirutana A. Srikanchana

7. PERFORMING ORGANIZATION NAME(S) AND ADDRESS(ES)
The Catholic University of America
Washington, D.C. 20064

E-Mail: 55srikan@pluto.ee.cua.edu

8. PERFORMING ORGANIZATION REPORT NUMBER

9. SPONSORING / MONITORING AGENCY NAME(S) AND ADDRESS(ES)
U.S. Army Medical Research and Materiel Command
Fort Detrick, Maryland 21702-5012

10. SPONSORING / MONITORING AGENCY REPORT NUMBER

11. SUPPLEMENTARY NOTES

12a. DISTRIBUTION / AVAILABILITY STATEMENT
Approved for Public Release; Distribution Unlimited

12b. DISTRIBUTION CODE

13. ABSTRACT (Maximum 200 Words)

Effective computational tools are developed for improved detection, diagnosis, and monitoring of breast cancer. A tactile mapping device (TMD) is tested for the early detection of breast cancer through more objective and quantitative breast palpation. Following the detection of breast cancer, diagnosis of the breast is the next step. We introduce a hybrid source decomposition algorithm, which allows for a computational characterization of tumor microvascular heterogeneity in both spatial and temporal domains. The goal is to reveal temporal-spatial patterns for the visualization and quantification of tumor-induced angiogenesis and response to therapy using dynamic contrast-enhanced magnetic resonance imaging (DCE-MRI). An image-based change detection approach is proposed to assess tumor's response to therapy. Based on promising experimental results, we anticipate that functional imaging based computational characterization of tumor heterogeneity and response will be useful in a wide variety of medical imaging studies.

14. SUBJECT TERMS
Breast Cancer

15. NUMBER OF PAGES
33

16. PRICE CODE

17. SECURITY CLASSIFICATION OF REPORT	18. SECURITY CLASSIFICATION OF THIS PAGE	19. SECURITY CLASSIFICATION OF ABSTRACT	20. LIMITATION OF ABSTRACT
Unclassified	Unclassified	Unclassified	Unlimited

Table of Contents

INTRODUCTION:

Effective computational tools are developed for improved detection, diagnosis, and monitoring of breast cancer. A tactile mapping device (TMD) is tested for the early detection of breast cancer through more objective and quantitative breast palpation. Following the detection of breast cancer, diagnosis of the breast is the next step. We introduce a hybrid source decomposition algorithm, which allows for a computational characterization of tumor microvascular heterogeneity in both spatial and temporal domains. The goal is to reveal temporal-spatial patterns for the visualization and quantification of tumor-induced angiogenesis and response to therapy using dynamic contrast-enhanced magnetic resonance imaging (DCE-MRI). An image-based change detection approach is proposed to assess tumor's response to therapy. Based on promising experimental results, we anticipate that functional imaging based computational characterization of tumor heterogeneity and response will be useful in a wide variety of medical imaging studies.
Our considerable efforts in the past year are:

- To construct training and testing databases of tactile mapping images and associated data.
- To construct MR modeling of tumor to estimate and tract changes of the tumor across time.
- To evaluate the performance of the TMD+NN in diagnosis and monitoring in terms of sensitivity to changes and reproducibility to measurements.

BODY:

In the first year of this award, we have fully demonstrated the feasibility of the tactile mapping device (TMD) for improving breast cancer examination technique in diagnosis, documentation, and training. In particular, the results have shown that new tactile mapping technology can quantitatively measure the location and applied forces in breast palpation, and the tactile features of detected breast lumps. The prototype interactive training program can track finger motions and applied forces during breast palpation in which on-line feedback can help the training to better understand the search strategy and adjust applied force level to increase the sensitivity.

In the second year of this award, we have integrated the tactile sensing technology and the vision-based neural network for investigations of soft tissue interactions with the tactile/force sensor. With the proven power of nonlinear signal processing both convolution neural network (CNN) and multi-layer perceptron (MLP) can be sued to characterized the hard inclusion (breast cancer) through neural network learning capabilities, instead of using a simplified complex biomechanics model with many heuristic assumptions. The tactile mapping systems using the neural networks and tactile sensing array can extract invariant parameters associated with the lesions (i.e., the size and depth of the lesion) can be estimated more accurately than those by the conventional approaches.

Following the detection of breast cancer, diagnosis of the breast is the next step. Recently, there has been a need to stimulate the development of novel imaging technologies that exploit our current knowledge of the genetic and functional bases of environmentally induced diseases and cancers. Such functional imaging capabilities will allow for the visualization and explanation of important disease-causing physiological and functional processes in the living tissue. Therefore, the potential of medical imaging to improve cancer treatment extends well beyond using imaging information to help select effective preventatives or treatments.

Dynamic contrast-enhanced magnetic resonance imaging (DCE-MRI) has been developed to provide additional functional information about tumor [1]. The technique has emerged as an effective tool to access tumor vascular characteristics, which can be used for measuring tissue perfusion, microvessel permeability, and vascular volume. The imaging technique has provided the information needed for diagnosis and treatment based on tumor location, size, and spread. It is also known that the kinetic characteristic changes following treatment have correlated with histopathological outcome (e.g., tumor blood volume, vascular permeability, and tumor perfusion) and patient survival. However pathology reveal distinct heterogeneity within and among tumors, that suggesting the need for individualize diagnosis and treatment to the unique characteristics of each specific case. Thus, dynamic measurements, in which the uptake and washout of contrast in tissues is monitored with time, can assist in the diagnosis of breast tumors and can provide information on vascular permeability and perfusion. The techniques are being applied to assess/monitor the response to treatment, which can be used to characterize microvasculature providing information about tumor microvessel structure and function.

However, widespread success of DCE-MRI may be limited by the need for the further development of technology, particularly due to the lacking of quantitative and computational data analysis tools included by the instruments [1]. Therefore, an effective computational data analysis technique for image-based lesion characterization of the vascularlity patterns (fast-/slow-flow kinetic) in functional imaging will provide richer diagnostic information, thus improve the sensitivity (e.g., signal-to-noise ratio) and specificity (e.g., heterogeneity) for early disease detection/diagnosis and monitoring of therapeutic response. The techniques are mainly used for the prognosis in breast cancer, and it also shows more promising for assessing the response to therapy. Subsequently, functional imaging will play an important role in the early detection, diagnosis, and treatment of diseases [2].
In this research, we introduced a hybrid decomposition algorithm, which allows for a computed simultaneous imaging of multiple biomarkers. The method is based on a combination of time-activity curve clustering, pixel subset selection, and independent component analysis. We demonstrate the principle of the approach on an image data set, and we then apply the method to the tumor vascular characterization using DCE-MRI.

Major portions of the work were reported in our manuscripts submitted to the *SPIE's medical imaging conference* and *NNSP 2003 conference.* [Attached]

KEY RESEARCH ACCOMPLISHMENTS:

Our key goal of Task II is to develop a neural network based intelligence system that estimates and track the changes (in size and depth) of tumors over time after diagnosis and during treatment. Furthermore, the MR modeling of tumor to estimate and track changes of the tumor across time in diagnosis and treatment is presented. Our accomplishments are the following:

- We have developed neural network training algorithms and computer interpretation codes, convolution neural network (CNN) based breast tumor characterization and parameter estimation.
- We have constructed the databases of tactile mapping images and the associated data for the training and testing of our neural network algorithms.
- We have developed a hybrid source decomposition algorithm, which allows for a computational characterization of tumor microvascular heterogeneity in both spatial and temporal domains. The goal is to reveal temporal-spatial patterns for the visualization and quantification of tumor-induced angiogenesis and response to therapy using dynamic contrast-enhanced magnetic resonance imaging (DCE-MRI).

REPORTABLE OUTCOMES:

- R. Srikanchana, Functional Imaging and Analysis of Tumor Heterogeneity by Cluster and Independent Component Analysis, Doctoral dissertation, The Catholic University of America, 2003.
- Y. Wang, J. Zhang, R. Srikanchana, J. Xuan, Z. Wang, Z. Szabo, Z. Bhujwalla, P. Choyke, K. Li, "Computed Simultaneous Imaging of Multiple Biomarkers," *Proc. IEEE Neural Networks for Signal Processing,* 2003.

- J. Zhang, R. Srikanchana, J. Xuan, K. Li, Y. Wang "Partially-Independent Component Analysis for Molecular Imaging," *SPIE's Intl. Symp. Medical Imaging,* vol. 5032, San Diego, CA, February 2003

- Presented the paper "Partially-Independent Component Analysis for Molecular Imaging," *SPIE's Intl. Symp Medical Imaging,* San Diego, CA, Feb. 2003.

CONCLUSIONS:

In this research, effective computational tools are developed for improved detection, diagnosis, and monitoring of breast cancer and response to therapy. We have demonstrated the principle of the approaches on both simulated and real data sets. Based on promising experimental results, we anticipate that functional imaging based computational characterization of tumor heterogeneity and response will be useful in a wide variety of medical imaging studies.

The main contribution of this research have shown that the TMD with associated new tools will improve physical breast examination in the ability to detect small tumors in breast palpation and increase the accuracy of early detection, leading to improved diagnosis and a reduction in breast cancer mortality. We have adapted new tactile mapping technology to the needs of improving physical breast examination and gather preliminary clinical data. We have conducted a study to advance fundamental understanding of palpation and solve these practical problems through the creation of a new TMD. This device measured three key variables during palpation: the examiner's search patterns, the applied forces, and the small-scale pressure variations at the skin due to lumps. A preliminary TMD prototype demonstrated the feasibility and effectiveness.

We have heavily focused on the DCE-MRI based angiogenesis imaging to elucidate two main challenging aspects (tumor heterogeneity and composite signals) in data analysis of functional imaging. Complementary to various existing methods (e.g., compartment modeling, factor analysis), we introduced a hybrid source decomposition algorithm, which allows for a computational characterization of tumor microvascular heterogeneity in both spatial and temporal domains. The method is based on a combination of time-activity curve clustering, pixel subset selection, and independent component analysis. The goal is to reveal temporal-spatial patterns for the visualization and quantification of tumor-induced angiogenesis and response to therapy using DCE-MRI of breast cancer. As a result, spatial distribution of tumor blood volume, vascular permeability, and tumor perfusion, as well as their TACs are simultaneously estimated, which closely resemble the expected characteristics of the tumor heterogeneity. The method can be used to

evaluate tumor angiogenesis inhabitation for cancer therapy and monitor the kinetic characteristic response to the anti-angiogenic following the treatment. The method consists of two major steps: (1) a multivariate cluster analysis for the initialization of the factor image decomposition; (2) a factor image decomposition by a partially-independent component analysis

We wish to suggest that our preliminary studies indicated a promising utility of hybrid blind source separation techniques in computed simultaneous imaging of multiple biomarkers. Although the optimality of this method may be data-dependent, we would expect it to be an effective tool applicable to various modalities.

REFERENCES

1) J. M. Hoffman and A. E. Menkens, "Molecular imaging in cancer: future directions and goals of the National Cancer Institute," *Acad. Radiol.*, vol. 7, pp. 905-907, 2000.
2) J. Evelhoch and S. Riederer, "Dynamic contrast-enhanced MRI," Workshop Report, National Cancer Institute, Mar. 19, 2001. (http://www3.cancer.gov/bip/DCEMRIrpt.htm)
3) American Cancer Society, *Cancer Facts and Figures*, Technical Report, 1994.
4) Feig SA. Screening guidelines and controversies. In Bassett LW, Jackson VP et al. Diagnosis of Diseases of the Breast. pp 329-343. WB Saunders Co, Philadelpia 1997
5) Tabar L, Fagerberg G, Duffy SW, et al. Update of the Swedish two-county program of mammographic screening for breast cancer. Radiologic Clinicsl of NA, 1992. 30: 187-210.
6) Society of Surgical Oncology Practice Guidelines. Breast cancer surgical practice guidelines. Oncology. 1997. 11: 877-886,
7) Rimer BK. Breast Cancer Screening. In Harris JR, Lippman ME, Morrow M, Hellman S. Diseases of the Breast. 1996. Pp 307-322.
8) Geng, J, "Rainbow 3D Camera - A New Concept for High Speed and Low-Cost 3D Vision", *Journal of Optical Engineering* Vol.35, No.2, p376, Feb 1996.
9) Wang Y, Nguyen C, Srikanchana R, Geng J, and Freedman MT, "Tactile mapping of palpable abnormalities for breast cancer diagnosis," *Proc. IEEE Conf. Robotics and Automation*, Detroit, 1999.
10) R. Srikachana, Y. Wang, C. Nguyen, and M. T. Freedman, "Soft Tissue Modeling in Palpable Lesion Characterization by Tactile Mapping Neural Networks," to appear *Proc. Intl. Joint Congress Neural Nets*, 1999.
11) Zeng J, Wang Y, Freedman MT, and Mun SK, "Finger tracking for breast palpation quantification using color image features," *Journal of Optical Engineering*, 36(12): 3455-3461, December 1997.
12) Y. Wang, S-H Lin, H. Li, and S-Y Kung, "Data Mapping by Probabilistic Modular Networks and Information Theoretic Criteria," *IEEE Transactions on Signal Processing*, vol. 46, no.12, pp. 3378-3397, December 1998.
13) Y. Wang and J. M. Morris, "On Numerical Verification of Time-Domain Moment Method in Ultrasound Tomography," *SPIE Journal of Biomedical Optics,* vol. 1, No. 3, pp. 324-329, July 1996.
14) Y. Wang and T. Adali, "Probabilistic neural networks for parameter quantification in medical image analysis," in *Biomedical Engineering Recent Development*, pp.669-672, J. Vossoughi, Editor, 1994.
15) Adames CK, Hall DC, Stein GH, Stephenson HS, Goldstein MK, and Pennypacker HS, "Lump detection in simulated human breasts," *Perception and Psychophysics*, 20(3), pp.163, 1976.
16) Dario, P and Bergamasco, M, "An advanced robot system for automated diagnosis tasks through palpation," *IEEE Trans. Biomed. Eng.*, vol. 35, no. 2, pp.118-126, February 1988.
17) Fearing, RS, "Tactile sensing mechanisms," *Intl. J. Robotics Research*, 9(3): 3-23, 1990.

18) Fletcher SW, O'Malley MS, and Bunce LA, "Physician's abilities to detect lumps in silicone breast models," *JAMA*, 253(15):2224-2228, 1985.
19) Howe, RD, Peine WJ, Kontarinis, DA, Son, J, "Remote palpation technology," *IEEE Engineering in Medicine and Biology*, 14(3): 318-323, May/June 1995.
20) Wellman, PS, "A biomechanical model for tactile mapping of palpable abnormalities," Harvard Robotics Lab Technical Report 96-002, Harvard University, 1996.
21) Gaston MH and Moody LE, "Improving utilization of brest and cervical cancer screening in your office practice," *Journal of National Medical Association*, 87(9): 700-704, 1995.
22) Foster RS, Worden JK, Costanza MC, and Solomon LJ, " Clinical breast examination and breast self-examination: past and present effect on breast cancer survival," *Cancer*, 69(7): 1992-1998, 1992.
23) American Cancer Society Brochure F-362, *How to Examine Your Breasts*, 1994.
24) J. Ophir, I. Cespedes, H. Ponnekanti, Y. Yazdi, and X. Li, "Elastography: a quantitative method for imaging the elasticity of biological tissues," *Ultrasonic Imaging*, 13:111-134, 1991.
25) C. D. Haagensen, *Physicians' Role in the Detection and Diagnosis of Breast Disease: Palpation of the Breast, Diseases of The Breast*, 3rd ed. Philadelphia: Saunders, pp.521-527, 1986.
26) H. S. Bloom et als., "Major stimulus dimensions determining detection of simulated breast lesions," *Perception and Psychophysics*, Vol. 32, pp. 251-260, 1982.
27) D. C. Hall, C. K. Adams, G. H. Stein, H. S. Stephenson, M. K. Goldstein, and H. S. Pennypacker, "Improved Detection of Human Breast Lesions," *Cancer*, Vol. 46, pp. 400-413, July 1980.
28) B. P. Haughey, J. R. Marshall, C. Mettlin, T. Nemoto, K. Kroldart, and M. Swanson, "Nurse's Ability to Detect Nodules in Silicone Breast Models," *Oncology Nursing Forum*, Vol. 11, No. 1, pp. 37-42, 1984.
29) M. S. O'Malley and S. W. Fletcher, "Screening for Breast Cancer With Breast Self-Examination A Critical Review," *JAMA*, Vol. 257, No. 16, pp. 2197-2203, 1987.
30) R. D. Howe, "Touch sensing and display for surgical applications," robotics, Vol. 4, No. 1, 1995.
31) R. D. Howe et als., "A tactile sensing and display system for teleoperated manipulation," *Proc. IEEE Intl. Conf. Robotics Auto.*, pp. 641-646, Nagoya, Japan, May 1995.
32) R. S. Fearing and J. M. Hollerbach, "Basic solid mechanics for tactile sensing," *Intl. J. Robotics Research*, 4(3): 40-54, Fall 1985.
33) J. M. Rehg and T. Kanade, "Visual tracking of high DOF articulated structures: an application to human hand tracking," *Proc. 3th European Conf. Computer Vision*, 1994.
34) T. Darrell and A. Pentland, "Space-time gestures," *Proc. IEEE Conf. Computer Vision and Pattern Recognition*, 1993.

APPENDICES:

Y. Wang, J. Zhang, R. Srikanchana, J. Xuan, Z. Wang, Z. Szabo, Z. Bhujwalla, P. Choyke, K. Li, "Computed Simultaneous Imaging of Multiple Biomarkers," *Proc. IEEE Neural Networks for Signal Processing,* 2003.

J. Zhang, R. Srikanchana, J. Xuan, K. Li, Y. Wang "Partially-Independent Component Analysis for Molecular Imaging," *SPIE's Intl. Symp. Medical Imaging,* vol. 5032, San Diego, CA, February 2003

Proc. IEEE Neural Networks for Signal Processing,
September 2003.

COMPUTED SIMULTANEOUS IMAGING OF MULTIPLE BIOMARKERS

Yue Wang Jianhua Xuan Rujirutana Srikanchana Junying Zhang
Zsolt Szabo Zaver Bhujwalla Peter Choyke King Li
Department of Electrical & Computer Engineering, Virginia Polytechnic Institute and State University, Alexandria, VA 22314 USA
Department of Electrical Engineering & Computer Science, The Catholic University of America, Washington, DC 20064 USA
Department of Radiology and Radiological Science, Johns Hopkins Medical Institutions, Baltimore, MD 21250 USA
Imaging Science and Diagnostic Radiology Division, National Institutes of Health, Bethesda, MD 20892 USA

Abstract. **Functional-molecular imaging techniques promise powerful tools for the visualization and elucidation of important disease-causing physiologic-molecular processes in living tissue. Most applications aim to find temporal–spatial patterns assocaited with different disease stages. When multiple agents are used, imagery signals often represent a composite of more than one distinct source due to functional-molecular biomarker heterogeneity, independent of spatial resolution. We therefore introduce a hybrid decomposition algorithm which allows for a computed simultaneous imaging of multiple biomarkers. The method is based on a combination of time-activity curve clustering, pixel subset selection, and independent component analysis. We demonstrate the principle of the approach on an image data set, and we then apply the method to the tumor vascular characterization using dynamic contrast-enhanced magnetic resonance imaging and brain neuro-transporter imaging using dynamic positron emission tomography.**

INTRODUCTION

With rapid advances recently made in developing molecular/functional-targeted contrast agents, ligands and imaging probes, new molecular or functional imaging techniques promise powerful tools for the visualization and elucidation of important disease-causing physiologic and molecular processes in living tissue [1, 2]. For example, dynamic contrast-enhanced magnetic resonance imaging (DCE-MRI) utilizes various molecular weight contrast agents to access, non-invasively, tumor microvascular characteristics. The extravas-

cular retention of intravenous contrast medium correlates to accumulation at sites of concentrated angiogenesis mediating molecules or microvessels (permeability). Kinetic (perfusion) changes following treatment have correlated with histopathological outcome and patient survival, and shall potentially be able to assess or predict the response to treatment particularly when using anti-angiogenic drugs [2]. On the other hand, positron emission tomography (PET) utilizes molecular probes (e.g, ligands for receptors or substrates for intracellular enzymes) labeled with positron-emitting radioisotopes. Tracer quantities yield a tomographic image after their retention, as a consequence of either specific ligand-receptor binding or conversion of substrate to "trapped" metabolic product(s) [1]. Fig. 1 shows the breast tumor images obtained by DCE-MRI.

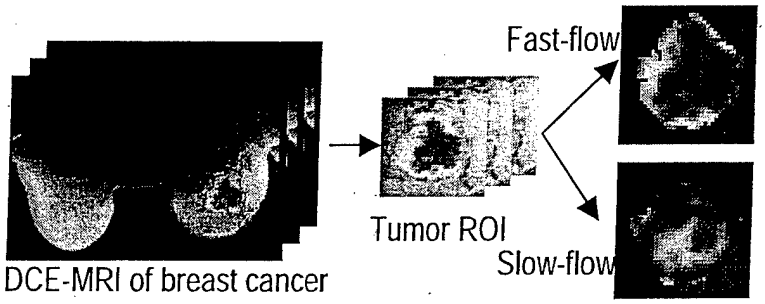

Figure 1: Images of advanced breast tumor obtained by DCE-MRI, where tumor-induced microvascular permeabilities, associated with different perfusion rate, reveal interesting spatial heterogeneous patterns.

As a common feature in functional or molecular imaging, pixels represent a composite of more than one distinct biomarker, independent of the spatial resolution. For example, DCE-MRI reveals heterogeneous mixture of tumor microvessels associated with different perfusion rate (e.g., fast vs. slow flow), and PET imaging of the neuro-transporters in the brain indicates that although highly sensitive to its target, the nonspecific binding of the radioligand is significant. As a result, the overlap of multiple biomarkers can severely decrease the sensitivity and specificity for the measurement of functional or molecular signatures associated with different disease processes.

Two most popular methods that aim to extract the images of individual biomarkers are compartment modeling and factor analysis [3]. Fig. 2 shows macroscale kinetics of probe-biomarker interactions. Compartment modeling can find time-activity curves (TACs) which are functionally meaningful, but requires pre-acquired input function and does not generally provide any spatial information about different tissue kinetics [3]. Factor analysis can find both factor images and TACs including the input function blindly, but may result in the factor images or TACs that are not unique or functionally meaningful [4]. Several blind compartment modeling methods were recently proposed, where the major concern is the parameter identifiability [5].

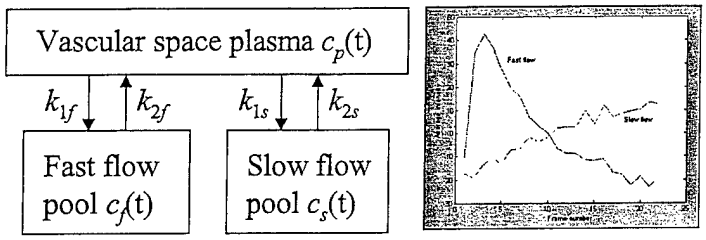

Figure 2: Illustration of two-tissue compartmentl model and time-activity curves.

In this paper, we introduce a hybrid decomposition algorithm which allows for a computed simultaneous imaging of multiple biomarkers. The method is based on a combination of time-activity curve clustering, pixel subset selection, and independent component analysis. We demonstrate the principle of the approach on an image data set, and we then apply the method to the tumor vascular characterization using DCE-MRI and brain neuro-transporter imaging using dynamic PET.

THEORY AND METHOD

Factored Compartment Model

We first introduce a simple form of linear factored compartment model and discuss its application to simultaneous biomarker imaging. On the basis of Fig. 2, tracer characterization within a region of interest (ROI) leads to a set of first order differential equations:

$$\begin{array}{rcl} \dot{c_f}(t) & = & k_{1f}c_p(t) - k_{2f}c_f(t) \\ \dot{c_s}(t) & = & k_{1s}c_p(t) - k_{2s}c_s(t) \\ c_m(t) & = & c_f(t) + c_s(t) + c_p(t) \end{array} \quad , \quad \begin{array}{rcl} c_f(t) & = & k_{1f}c_p(t) \circledast e^{-k_{2f}t} \\ c_s(t) & = & k_{1s}c_p(t) \circledast e^{-k_{2s}t} \end{array} \qquad (1)$$

where $c_f(t)$ and $c_s(t)$ are the tissue activity in the fast turnover and slow turnover pools, respectively, at time t; $c_p(t)$ is the tracer concentration in plasma (i.e., the input function); $c_m(t)$ is the measured total tissue activity; k_{1f} and k_{1s} are the unidirectional transport constants from plasma to tissue (permeability in ml/min/g: spatially-varying); k_{2f} and k_{2s} are the rate constants for efflux (perfusion in /min: spatially-invariant), and $\circledast$ denotes the mathematical convolution. Note that $c_f(t)$, $c_s(t)$, $c_p(t)$, and $c_m(t)$ are called the *time-activity curves* (TACs).

Linear system theory suggests a simple method to convert temporal kinetics to spatial information [6]. Let $k_{1f}(i)$ and $k_{1s}(i)$ be the local permeability parameters associated with pixels $i = 1, ..., N$, i.e., the permeability of fast and slow turnover (perfusion) regions in the pixel, respectively, and $v_p(i)$ be the plasma volume in tissue. The measured pixel TAC $c_m(i,t)$ is [2]

$$c_m(i,t) = k_{1f}(i)c_p(t) \circledast e^{-k_{2f}t} + k_{1s}(i)c_p(t) \circledast e^{-k_{2s}t} + v_p(i)c_p(t) \qquad (2)$$

that leads to a factored compartment model [4]

$$\begin{bmatrix} c_m(i,t_1) \\ c_m(i,t_2) \\ \cdot \\ \cdot \\ \cdot \\ c_m(i,t_n) \end{bmatrix} = \begin{bmatrix} c_p(t_1) \circledast e^{-k_{2f}t_1} & c_p(t_1) \circledast e^{-k_{2s}t_1} & c_p(t_1) \\ c_p(t_2) \circledast e^{-k_{2f}t_2} & c_p(t_2) \circledast e^{-k_{2s}t_2} & c_p(t_2) \\ \cdot & \cdot & \cdot \\ \cdot & \cdot & \cdot \\ \cdot & \cdot & \cdot \\ c_p(t_n) \circledast e^{-k_{2f}t_n} & c_p(t_n) \circledast e^{-k_{2s}t_n} & c_p(t_n) \end{bmatrix} \begin{bmatrix} k_{1f}(i) \\ k_{1s}(i) \\ v_p(i) \end{bmatrix} \tag{3}$$

where $\mathbf{A}= [\ c_p(t) \circledast e^{-k_{2f}t} \quad c_p(t) \circledast e^{-k_{2s}t} \quad c_p(t)\ ]$ is called mixing matrix consisting of the TACs associated with underlying factor images whose least square estimates are

$$\begin{bmatrix} k_{1f}(i) \\ k_{1s}(i) \\ v_p(i) \end{bmatrix} = \left(\mathbf{A}^T\mathbf{A}\right)^{-1}\mathbf{A}^T \begin{bmatrix} c_m(i,t_1) \\ c_m(i,t_2) \\ \cdot \\ \cdot \\ \cdot \\ c_m(i,t_n) \end{bmatrix}. \tag{4}$$

Below we propose three different approaches that aim to reconstruct the factor images for the cases of multi-region insignificantly-overlapped, single-region significantly-overlapped, and multi-region significantly-overlapped, heterogeneities.

Multivariate Cluster Analysis

Biomarker heterogeneity in space motivates a natural consideration of multivariate cluster analysis (i.e., pixel TAC classification) for factor image decomposition. Since vascular space $c_p(t)$ is usually very high in the early time-course and dropped quickly (e.g., delta function), our initial analysis focuses on the tissue perfusion activities. Ideally, when there are only pure-volume pixels, i.e., $[\ k_{1f}(i) \quad k_{1s}(i)\ ]^T$ has only one nonzero element, there shall be a one-to-one mapping between pixel TAC $c_m(i,t)$ and factor TAC $c_f(t)$ or $c_s(t)$ except for an arbitrary scaling and noise effect.

Since the *shape* rather than the magnitude of the pixel TAC $c_m(i,t)$ is of the interest, we perform "centering" and "normalization" on each pixel TAC $c_m(i,t)$ over time t to a constant scale with mean zero

$$c_m^*(i,t) = \left[c_m(i,t) - \frac{1}{n}\sum_{j=1}^{n} c_m(i,t_j)\right] / \sigma_{c_m(i)} \tag{5}$$

where $\sigma_{c_m(i)}$ is the standard deviation of $c_m(i,t)$ over t. We have

$$c_m^*(i,t) = k_{1f}^*(i)c_f^*(t) + k_{1s}^*(i)c_s^*(t),\ k_{1f}^*(i) + k_{1s}^*(i) = 1 \tag{6}$$

where each of $\{k_{1f}^*(i),\ k_{1s}^*(i),\}$ can take on any value in the range $(0,\ 1)$ subject to the noise effort. Assume that the noise effect is approximately gaussian,

the pixel TAC $c_m^*(i,t)$ can be represented by a gaussian random vector $\mathbf{c}_m^*(i)$ with mean $\mu_{f,s}$ and covariance matrix $\mathbf{C}_{f,s}$. There has been considerable success in using the standard finite normal mixture (SFNM) distribution to adequately model clustered data set, taking a sum of the following general form [7]

$$p(\mathbf{c}_m^*) = \pi_f g(\mathbf{c}_m^*|\mu_f, \mathbf{C}_f) + \pi_s g(\mathbf{c}_m^*|\mu_s, \mathbf{C}_s) \tag{7}$$

where $\pi_{f,s}$ is the corresponding mixing proportion, with $0 \leq \pi_{f,s} \leq 1$ and $\pi_f + \pi_s = 1$, and g is the gaussian kernel.

The maximum likelihood estimation of the SFNM model can be performed by the expectation-maximization (EM) algorithm. We have previously developed a VISual Data Analyzer (VISDA) to perform multivariate cluster analysis [7, 8]. The procedure using VISDA provides "soft" splits of the pixel TAC vectors, hence allowing the pixel TACs $c_m(i,t)$ to contribute simultaneously to the multiple factor TACs. Specifically, the outcome of such a multivariate cluster analysis is the posterior Bayes probabilities of pixel i associated with $c_{f,s}(t)$

$$z_{i(f,s)} = \frac{\pi_{f,s} g(\mathbf{c}_m^*(i)|\mu_{f,s}, \mathbf{C}_{f,s})}{\sum \pi_{f,s} g(\mathbf{c}_m^*(i)|\mu_{f,s}, \mathbf{C}_{f,s})} \tag{8}$$

that leads to

$$c_f(t) = \sum_{i=1}^{N} z_{if} c_m(i,t) \text{ and } c_s(t) = \sum_{i=1}^{N} z_{is} c_m(i,t). \tag{9}$$

Having determined the factor TACs $\mathbf{A}$= [$c_f(t)$ $c_s(t)$], the factor images k= [$k_{1f}(i)$ $k_{1s}(i)$]^T will be reconstructed from $c_m(i,t)$ according to Eq. 4. However, pixels called *partial-volume pixels* represent a combination of factor TACs due to the *partial-overlap* of the factor images in space. The partial-volume effect can be, fortunately, solved by an appropriate partial-volume modeling [9]. Let $c_{fs}(t)$ be the TAC of the partial-volume pixels. Based one the derivation in [9], we can write a SFNM model that includes partial-volume effect as

$$\begin{aligned} p(\mathbf{c}_m^*) &= \pi_f g(\mathbf{c}_m^*|\mu_f, \mathbf{C}_f) + \pi_s g(\mathbf{c}_m^*|\mu_s, \mathbf{C}_s) \\ &+ \pi_{fs} g\left(\mathbf{c}_m^* | \tfrac{1}{2}(\mu_f + \mu_s), \tfrac{1}{3}(\mathbf{C}_f + \mathbf{C}_s) + \tfrac{1}{12}(\mu_f - \mu_s)(\mu_f - \mu_s)^T\right) \end{aligned} \tag{10}$$

where $0 \leq \pi_{fs} \leq 1$ and $\pi_f + \pi_s + \pi_{fs} = 1$. We have modified the VISDA algorithm to estimate this *constrained* SFNM model. We will first apply unconstrained EM algorithm to classify pixel TACs into three clusters and then, identify two clusters with smallest covariances as those representing pure-volume pixels, and lastly re-estimate the model using a constrained EM algorithm. In M-step specifically, we will only *estimate* the parameters of pure-volume clusters using $z_{i(f,s)}$, and *assign* the parameter values for the partial-volume cluster. Once again, based on newly estimated factor TACs, the factor images are accordingly reconstructed.

Independent Component Analysis

For *single-region significantly-overlapped* cases, the similarity between Eq. 3 and latent variable modeling motivates the consideration of independent component analysis (ICA) approach [10]. As aforementioned, the factor images are not observable, and nothing is known about the properties of the TACs. In the absence of this information, one has to proceed "blindly" to recover the factor images from their TAC-modulated activity mixtures [4]. ICA method utilizes *independency* as a guiding principle and performs a *nongaussian* factor analysis leading to a unique solution [11]. More precisely, by assuming that the hidden components are statistically independent with nongaussian distributions, these hidden sources can be found by ICA, except for an arbitrary scaling of each signal component and permutation of indices. ICA approach exploits primarily *temporal diversity* in that the dynamic images taken at different times carry different mixtures of the factor images [4].

Specifically, let demixing matrix $\mathbf{W}$ be an estimate that gives a good approximation of the inverse of $\mathbf{A}$, then according to the *Central Limit Theorem* that states "a sum of independent random variables usually has a distribution that is closer to gaussian than any of the original random variables," the recovered factor image

$$\mathbf{y}(i) = \mathbf{W}\mathbf{c}_m(i) = (\mathbf{WA})\mathbf{k}(i) \tag{11}$$

is usually more gaussian than any of $k_j(i)$ and becomes least gaussian when it in fact equals one of the $k_j(i)$, i.e., each row or column of $\mathbf{WA}$ has only one nonzero element where $\mathbf{W}=\mathbf{PDA}^{-1}$ with $\mathbf{P}$ and $\mathbf{D}$ being permutation and scaling matrices. Thus, maximizing the nongaussianity of the output signal $\mathbf{y}(i)$ produces the independent components, i.e., true $\mathbf{k}(i)$.

There are several ways for estimating the model of ICA including maximization of nongaussianity, maximum likelihood, and minimizing joint mutual information. Most estimation principles and objective functions are equivalent, at least in theory. Two popular and publicly available software codes are FastICA and RunICA algorithms. A thorough discussion on ICA theory can be found in a recent textbook [10].

Partially-Independent Component Analysis

For *multi-region significantly-overlapped* cases, we have found that direct application of ICA to factor image decomposition using all the pixels, however, often leads to an unsatisfactory recovery of $\mathbf{k}(i)$ [4]. This shall not be a surprise since a more reasonable assumption, suggested by underlying anatomy, is that the functional regions are piecewise homogeneous. This seemingly global viewpoint turns out to have important consequences, since it implies that the clustered joint distribution of the factor images exhibits only local independency between the functional regions and hence, does not assure the factor images to be globally independent [11]. Thus, we shall expect to achieve a better decomposition using a subset of pixels that corresponds to

a homogeneously-overlapped single-region and would be approximately independent.

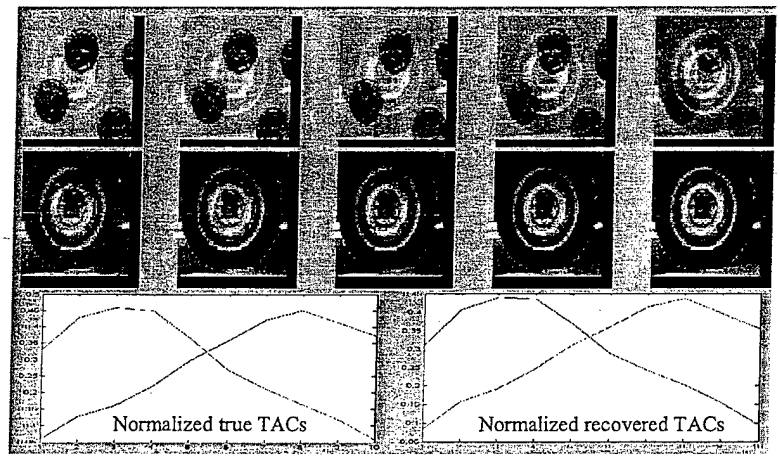

Figure 3: Simulated image sequence consisting of "tire" and "coin" objects. The mixing matrix resembles the typical shapes of fast and slow flows in DCE-MRI.

We therefore developed a partially-independent component analysis technique [4]. Rather than using all the pixels that give rise to a large separation error, we attempt to identify a homogeneously-overlapped single-region and over which to estimate the demixing matrix $\mathbf{W}$ and subsequently factor images $\mathbf{k}(i)$. Once again, the region identification can be, fortunately, solved by performing multivariate pixel-TAC clustering using VISDA software [7, 8]. Note that in the present case, all the pixels are homogeneously-mixed partial-volume pixels. Once all the homogeneously-overlapped individual regions are identified, we shall perform ICA over each of the individual pixel subsets and then take an averaged outcome of the factor images and TACs. The selection of homogeneous ROIs can be done by either visual inspection or using model selection criteria [7].

EXPERIMENTAL RESULT

We shall now illustrate the operation of our method when applied to a simple image data set, and then present results from the study of DCE-MRI and PET data sets. We first consider a digital image set consisting of ten observations generated from the mixtures of "tire" and "coin" images, see Fig 3. Experiments are conducted over several runs of the ICA and PICA algorithms, each with a different random mixing matrix. With an appropriate pixel selection, the estimated TACs are given against the true TACs in Fig. 3 (bottom row). In this experiment, the basic principle and capable nature of the PICA method are evident as the PICA, using only independent portion

of the observations, successfully separates two image patterns that have been insufficiently recovered by conventional ICA [4].

The second experiment reports the effectiveness of multivariate pixel TAC clustering for *multi-region insignificantly-overlapped* cases. The data set is obtained by DCE-MRI, see in Fig. 1. This is an advanced breast tumor case that shows significant vascular heterogeneity where the *biomarkers* are vascular permeability with fast and slow perfusions. The two-dimensional projection of the pixel TACs is given in Fig. 4 (left) and the estimated factor TACs are given in Fig. 4 (right). We noticed that the reconstructed factor images by multivariate cluster analysis paralleled the expected vascular distributions very nicely and many independent trials reached similar satisfactory results, see Fig. 1 (right column). Since this represents also a globally-dependent case, we have performed conventional ICA using all the pixels, not to our surprise, the unexpected overlaps become clearly visible.

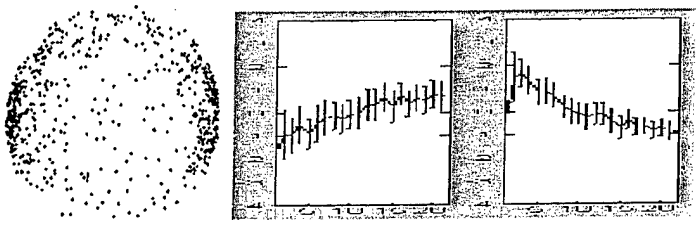

Figure 4: Normalized pixel TAC projection (left) and the corresponding factor TACs (right), obtained by VISDA software.

As an example of more challenging problems, we considered dynamic PET imaging of SERT using $C^{11}McN^{+}5652$. Images shown in Fig. 5 (top row) were obtained using a GE 4096 whole body scanner with 15 slices at the center of the field-of-view. The slice thickness is 6.5 mm and the spatial resolution is 6~7 mm. The images correspond to the 7th PET slice and were taken between 8 to 18 time snapshots in the sequence. Our preliminary results using PICA, shown in Fig. 5 (bottom row), were quite promising in that the extracted factors closely resemble the expected compartmental kinetics of the radioligand consistent with its pharmacology, and the factor images generated simultaneously reveal regional distribution of the specific (left) and nonspecific (right) binding sites. We believe that this experiment indicated a relatively successful application of PICA technique to neuro-transporter binding separation in PET, given the difficulty of the task.

Final experiment reports the results of multivariate clustering in blind estimation of both the input function and factor images (microvessel permeability associated with fast and slow perfusions-FP/SP). The separation of plasma space and fast perfusion permeability is expected challenging. We divided the TACs into two portions over time. We firstly estimated FP and SP TACs from the late portion of the TACs assuming insignificant presence of the input function. We then removed the pixels belonging to SP and es-

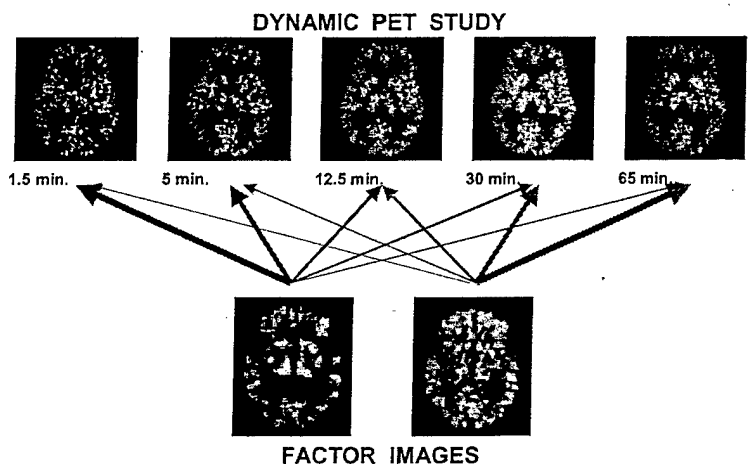

Figure 5: Dynamic PET images of the brain and the reconstructed factor images that represent the specific and non-specific binding sites (2 biomarkers of interest).

timated the input function from the early portion of the TACs where the FP was initialized by the outcomes of the preceding step. The results are given in Fig. 6. The processed data sets are insufficient for a rigorous test of our method. So far as we can tell, it is roughly compatible with the clinical expectations, but it must be regarded as unproved until it has been checked against more realistic truth.

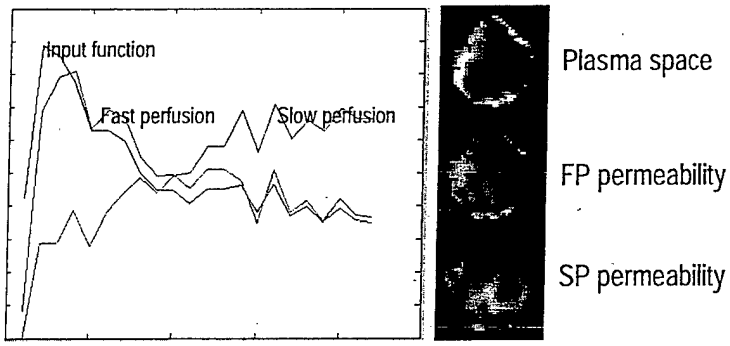

Figure 6: Blindly estimated input function & factor images by pixel TAC clustering.

DISCUSSION

We wish to suggest that our preliminary studies indicated a promising utility of hybrid blind source separation techniques in computed simultaneous

imaging of multiple biomarkers. Although the optimality of this method may be data-dependent, we would expect it to be an effective tool applicable to various modalities. We are currently investigating further application of non-negative matrix factorization [12] and separation by non-negative reverse correlation analysis, where the central idea is to relax both the independence and nongaussian assumptions.

ACKNOWLEDGEMENT

This work was supported in part by the Department of Defense under Grant DAMD17-98-8045 and the National Institutes of Health under Grant AG14400.

REFERENCES

[1] S. S. Gambhir, E. Bauer, M. E. Black, Q. Liang, M. S. Kokoris, J. R. Barrio, M. Lyer, M. Namavari, M. E. Phelps, and H. R. Herschman, "A mutant herpes simplex virus type 1 thymidine kinase reporter gene shows improved sensitivity for imaging reporter gene expression with positron emission tomography," *Proc. Natl. Acad. Sci.*, vol. 97, no. 6, pp. 2785-2790, March 2000.

[2] Y. Zhou, S-C Huang, T. Cloughesy, C. K. Hoh, K. Black, and M. E. Phelps, "A modeling-based factor extraction method for determining spatial heterogeneity of Ga-68 EDTA kinetics in brain tumors," *IEEE Trans. Nuclear Sci.*, vol. 44, no. 6, pp. 2522-2527, Dec. 1997.

[3] L. Cinotti, J. P. Bazin, R. DiPaola, H. Susskind, and A. B. Brill, "Processing of Xe-127 regional pulmonary ventilation by factor analysis and compartmental modeling," *IEEE Trans. Med. Imaging*, vol. 10, no. 3, pp. 437-444, 1991.

[4] Y. Wang, J. Zhang, K. Huang, J. Khan, and Z. Szabo, "Independent component imaging of disease signatures," *Proc. IEEE Intl. Symp. Biomed. Imaging*, pp. 178-181, July 7-10, Washington, DC 2002.

[5] K-P Wong, D. Feng, S. R. Meikle, and M. J. Fulham, "Simultaneous estimation of physiological parameters and the input function-in vivo PET data," *IEEE Trans. Info. Tech. Biomed.*, vol. 5, no. 1, pp. 67-76, Mar. 2001.

[6] W. J. Rugh, *Linear System Theory*, Prentice-Hall, Inc., 1996.

[7] Y. Wang, L. Luo, M. T. Freedman, and S-Y Kung, "Probabilistic principal component subspaces: A hierarchical finite mixture model for data visualization," *IEEE Trans. Neural Nets*, vol. 11, no. 3, pp. 625-636, May 2000.

[8] Z. Wang, Y. Wang, J. Lu, S-Y Kung, J. Zhang, R. Lee, J. Xuan, J. Khan, and R. Clarke, "Discriminatory mining of gene expression microarray data," *Journal of VLSI Signal Processing System*, 2003. in press

[9] P. Santago and H. D. Gage, "Statistical models of partial volume effect," *IEEE Trans. Image Processing*, vol. 4, no. 11, pp. 1531-1540, 1995.

[10] A. Hyvarinen, J. Karhunen, and E. Oja, *Independent Component Analysis*, New York: John Wiley, 2001.

[11] H. Attias, "Independent factor analysis," *Neural Computation*, vol. 11, pp. 803-851, 1999.

[12] D. D. Lee and H. S. Seung, "Learning the parts of objects by non-negative matrix factorization," *Nature*, vol. 401, pp. 788-791, October 1999.

SPIE's Intl. Symp. Medical Imaging
vol. 5032, San Diego, CA, February 2003

Partially-Independent Component Analysis of Tumor Heterogeneities By DCE-MRI

Junying Zhang[a], Rujirutana Srikanchana[a], Jianhua Xuan[a], Peter Choyke[b],

King Li[b], and Yue Wang[a]

[a]Department of Electrical Engineering and Computer Science,
The Catholic University of America, Washington, DC 20064, USA
[b]Diagnostic Radiology, National Institutes of Health, Bethesda, MD 20892, USA

ABSTRACT

Dynamic contrast enhanced magnetic resonance imaging (DCE-MRI) has emerged as an effective tool to access tumor vascular characteristics. DCE-MRI can be used to characterize microvasculature noninvasively for providing information about tumor microvessel structure and function (e.g., tumor blood volume, vascular permeability, and tumor perfusion). However, pixels of DCE-MRI represent a composite of more than one distinct functional biomarker (e.g., microvessels with fast or slow perfusion) whose spatial distributions are often heterogeneous. Complementary to various existing methods (e.g., compartment modeling, factor analysis), this paper proposes a blind source separation method that allows for a computed simultaneous imaging of multiple biomarkers from composite DCE-MRI sequences. The algorithm is based on a partially-independent component analysis, whose parameters are estimated using a subset of informative pixels defining the independent portion of the observations. We demonstrate the principle of the approach on simulated image data sets, and then apply the method to the tissue heterogeneity characterization of breast tumors. As a result, spatial distribution of tumor blood volume, vascular permeability, and tumor perfusion, as well as their time activity curves (TACs) are simultaneously estimated.

Keywords: Independent component analysis (ICA), partially-independent component analysis (PICA), intrinsic dependency/non-intrinsic dependency of the components, dynamic contrast-enhanced magnetic resonance imaging (DCE-MRI), compartment model, time activity curves (TACs).

1. INTRODUCTION

Remarkable advances in functional imaging have been made in developing molecular-targeted contrast agents, ligands and imaging probes. Such imaging capabilities will allow for the visualization and elucidation of important disease-causing physiologic and molecular processes in living tissue. Subsequently, functional imaging will play an important role in the early detection, diagnosis, and treatment of diseases.[1] It is known that most advanced tumors are highly heterogeneous in structure that may reflect the underlying angiogenesis and/or metastasis.[2] Dynamic contrast enhanced magnetic resonance imaging (DCE-MRI) is a noninvasive imaging method for tumor microvascular characterization, which can be applied to assess (and potentially predict) the response to treatment including anti-angiogenic drugs. Kinetic characteristics changes following treatment have correlated with histopathological outcome (e.g., microvessel density) and patient survival. However, widespread success of DCE-MRI may be limited by the need for further technology development, particularly due to the lacking of quantitative and computational data analysis tools included by the instruments.

As a common problem in functional imaging, pixels represent a composite of more than one distinct molecular marker (i.e., the observed pixel intensity will consist of the weighted sum of activities of the various molecules). This problem exists for various reasons, e.g., target mixture, probe non-specificity, and kinetics or spectrum overlap. These aspects are briefly described as follows. First, mixed signals can result when distinct markers are

Further author information: (Send correspondence to Rujirutana Srikanchana)
E-mail: 55srikanchan@cua.edu, Telephone: 1 202 319 5243
Address: EE/CS Department, The Catholic University of America, Washington, D.C., U.S.A.

combined into a homogeneous mixture (e.g., fast and slow flow microvessels), independent of spatial resolution. Second, ligand-receptor binding depends largely on the three-dimensional shapes of both elements, where a ligand has many bonds that can be rotated into many different positions resulting in many shapes. Third, even with a precision excitation source, any overlap of the absorption spectra of the fluorophores leads to the excitation of multiple fluorophores whose emission spectra often also overlap. Thus, the observed signal intensity may well be composed of the emission from several markers of differing concentration and kinetics/spectrum (e.g., specific/nonspecific bindings, fast/slow flows). As a result, the overlap of multiple molecular signatures can severely decrease the sensitivity and specificity for the measurement of molecular signatures associated with different disease processes. As an example, imaging neuro-transporters in the brain requires the passage of radioligands across the blood brain barrier by ways of their high lipophilicity. But lipophilicity carries the risk of high nonspecific binding and retention in the white matter and could result in a bias of the estimated kinetic parameters that are used to measure binding to specific recognition sites.

It is well known that Independent Component Analysis (ICA)[26,27] is a powerful method for blind source separation with a strong assumption that the sources are independent to each other. This paper describes a computation approach to dependent component imaging, where functional imaging is the case. The method is to identify an informative index subspace and over which to separate mixed imagery sources by partially-independent component analysis (PICA), whose parameters are estimated using informax principle. We discuss the theoretic roadmap of the approach, and its applications to computer simulation phantoms and DCE-MRI sequences of breast tumor.

2. THEORY AND METHOD

Independent component analysis (ICA)[26] is a statistical and computational technique for revealing hidden factors that underlie sets of random variables, measurements, or signals. The application of ICA has been found in many separate fields such as feature extraction, image processing, medical image processing, telecommunication, econometric signal processing, and so fourth.[11,27] The method aims at recovering the unobservable independent sources (or signals) from multiple observed data masked by linear or nonlinear mixing of the components.[27] One of the basic assumptions for ICA model is the statistical independence between components.[26] However, the dependent components are often occurred in the real world situation, including functional imaging derived from tissue samples.

2.1. Compartment Modeling

Compartment modeling forms the basis for tracer characterization in DCE-MRI.[3] Fig. 1 shows a parallel mode two-tissue compartment model.[2] The conventional compartment model leads to a set of first order differential equations:

$$\begin{array}{rcl} \dot{c_f}(t) & = & k_{1f}c_p(t) - k_{2f}c_f(t) \\ \dot{c_s}(t) & = & k_{1s}c_p(t) - k_{2s}c_s(t) \\ c_t(t) & = & c_f(t) + c_s(t) \\ c_m(t) & = & c_f(t) + c_s(t) + c_p(t) \end{array} \tag{1}$$

where $c_f(t)$ and $c_s(t)$ are the tissue activity in the fast turnover and slow turnover pools, respectively, at time t; $c_p(t)$ is the tracer concentration in plasma (i.e., the input function); $c_t(t)$ is the total tissue activity; $c_m(t)$ is the measured total tissue activity; k_{1f} and k_{1s} are the unidirectional transport constants from plasma to tissue (ml/min/g: spatially shift-varying); and k_{2f} and k_{2s} are the rate constants for efflux (/min: spatially shift-invariant). It is important to note that $c_f(t)$, $c_s(t)$, $c_p(t)$, and $c_m(t)$ are also called the *time-activity curves* (TACs) associated with a pre-defined region of interest (ROI).

It can be shown that $c_f(t)$ and $c_s(t)$ can be solved analytically in a parametric form

$$\begin{array}{rcl} c_f(t) & = & k_{1f}c_p(t) \otimes e^{-k_{2f}t} \\ c_s(t) & = & k_{1s}c_p(t) \otimes e^{-k_{2s}t} \end{array} \tag{2}$$

where $\otimes$ denotes the mathematical convolution operation. By fitting $c_m(t)$ to the measured ROI TAC in the light of pre-acquired $c_p(t)$, the model parameters (k_{1f}, k_{1s}, k_{2f}, k_{2s}) can be estimated.[3,4]

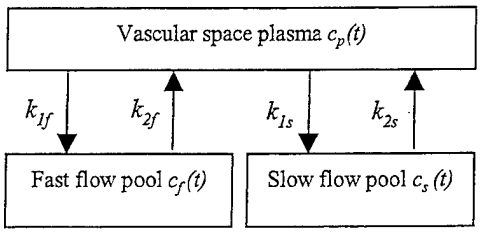

Figure 1. Two-tissue compartmant model (parallel mode).

Based on linear system theory, a simple method can be developed to convert temporal kinetics to spatial information.[2,5] First, we can normalize the ROI based tissue kinetics to define three TACs for each pixel

$$\begin{array}{rcccl} a_f(t) & = & \frac{c_f(t)}{k_{1f}} & = & c_p(t) \otimes e^{-k_{2f}t} \\ a_s(t) & = & \frac{c_s(t)}{k_{1s}} & = & c_p(t) \otimes e^{-k_{2s}t} \\ a_p(t) & = & \frac{c_p(t)}{v_p} & & \end{array} \tag{3}$$

where v_p is the plasma volume in tissue. Second, for pixels $i = 1, ..., N$ within an ROI, we let $k_{1f}(i)$ and $k_{1s}(i)$ be the local model parameters and use them to describe the dynamics of each pixel in the ROI

$$c_m(i,t) = k_{1f}(i)a_f(t) + k_{1s}(i)a_s(t) + v_p(i)a_p(t) \tag{4}$$

where $c_m(i,t)$ is the measured pixel TAC, $k_{1f}(i)$ and $k_{1s}(i)$ are the permeability of fast and slow turnover regions in the pixel, respectively, and $v_p(i)$ is the plasma volume in the pixel. We call this representation as factored compartment modeling.[5]

Third, let $(t_1, t_2, ..., t_n)$ be the sampling time points of the DCE-MRI measurements. Then, the linear least square solution of Eq. (4) can be given by the following equation:

$$\begin{bmatrix} k_{1f}(i) \\ k_{1s}(i) \\ v_p(i) \end{bmatrix} = \left(\mathbf{A}^T\mathbf{A}\right)^{-1}\mathbf{A}^T \begin{bmatrix} c_m(i,t_1) \\ c_m(i,t_2) \\ \cdot \\ \cdot \\ \cdot \\ c_m(i,t_n) \end{bmatrix} \tag{5}$$

where

$$\mathbf{A} = \begin{bmatrix} a_f(t_1) & a_s(t_1) & a_p(t_1) \\ a_f(t_2) & a_s(t_2) & a_p(t_2) \\ \cdot & \cdot & \cdot \\ \cdot & \cdot & \cdot \\ \cdot & \cdot & \cdot \\ a_f(t_n) & a_s(t_n) & a_p(t_n) \end{bmatrix}. \tag{6}$$

The estimated values of $k_{1f}(i)$, $k_{1s}(i)$ and $v_p(i)$ vary from pixel to pixel and reconstruct three factor images respectively. In particular, factor images $k_{1f}(i)$ and $k_{1s}(i)$ represent ROI sub-regions with fast and slow kinetics, respectively.

Preliminary effort has been recently made to perform blind compartment modeling without any knowledge of the input function.[12–15] An initial effort, eigenvector based multichannel blind deconvolution (EVAM),[16] was used to estimate the parameters of a two-tissue compartment model for PET FDG imaging,[12] but was shown to give relatively poor (sensitive to noise) and non-unique estimates in a simulation study.[13] A more optimal solution was proposed on the application of the iterative quadratic maximum-likelihood (IQML) method to parameter estimation.[13] The blind identification problem is treated as a nonlinear least square problem whose variables are separate.[17] Other approaches in which both the input function and kinetic parameters are treated as unknowns have been explored in [14, 15].

3. PARTIALLY-INDEPENDENT COMPONENT ANALYSIS (PICA)

3.1. Independent Component Analysis (ICA)

As aforementioned, one potential limitation associated with compartment analysis is that they are all restricted to a parametric (thus simplified) model that may not adequately describe the underlying physiological or biochemical processes about tracer-target interactions, in addition to the likely invasive acquisition of the input function. Although factor analysis (FA) attempts to solve the problem, the results were mostly unsatisfactory.

From linear system theory,[24] it can be shown that the solution (zero-state response) to a kinetic system has the very general form as shown in Eq. (4), or Eq. (7) as represented in vector-matrix form. This motivates the consideration of a statistically-principled computational approach involving newly invented independent component analysis (ICA) theory.[11,26,27] The goal is to blindly and computationally reconstruct both $\mathbf{A}$ and $\mathbf{k}$ based on $\mathbf{c}_m$. This philosophy for computed simultaneous imaging of multiple biomarkers is similar in spirit to the blind source separation (BSS) for solving the *cocktail-party problem*.[26]

From latent variable model interpretation,[28] Eq. (7)

$$\begin{bmatrix} c_m(i,t_1) \\ c_m(i,t_2) \\ \cdot \\ \cdot \\ \cdot \\ c_m(i,t_n) \end{bmatrix} = \mathbf{A} \begin{bmatrix} k_{1f}(i) \\ k_{1s}(i) \\ v_p(i) \end{bmatrix}, \tag{7}$$

describes how the observed data are generated by a process of mixing the latent (or "hidden") variables, where matrix $\mathbf{A}$ is called the *mixing matrix*, the factor images (or "source signals") are not observable, and nothing is known about the properties of the TACs (or "mixing process"). In the absence of this information, one has to proceed "blindly" to recover the factor images from their TAC-modulated activity mixtures.[5]

We can state such *computed simultaneous imaging of multiple biomarkers* as follows: "Given N independent realizations of the measured pixel TAC vector $\mathbf{c}_m(i,t)$, $i = 1,2,...,N$, find an estimate of the inverse of the TAC-mixing matrix $\mathbf{A}(t)$ and factor image vector $\mathbf{k}(i) = [k_{1f}(i), k_{1s}(i)]^T$."

ICA method, as a newly invented statistical and neural computation technique, promises a powerful computational tool for separating hidden sources from mixed signals when many classic methods fail completely.[26] ICA method utilizes *independence* as a guiding principle and performs BSS based on a *nongaussian* factor analysis with a unique solution.[11] More precisely, by assuming that the hidden components are statistically independent with nongaussian distributions, these hidden sources can be found by ICA, except for an arbitrary scaling of each signal component and permutation of indices. In other words, it is feasible to find a demixing matrix $\mathbf{W}$ whose individual rows are a rescaling and permutation of those of the mixing matrix $\mathbf{A}$. ICA approach exploits primarily *temporal diversity* in that the dynamic images taken at different times carry different mixtures of the factor images.[5] There are several algorithms for ICA that are derived from different optimization principles. More details can be found in [11, 26].

3.2. Partially-ICA

We have found that direct application of ICA to tumor heterogeneity characterization using all the pixels, however, often leads to an unsatisfactory recovery of factor images $\mathbf{k}(i)$. By a closer look at the joint distribution of the factor images, we found that they are often not statistically independent over the whole pixel set.[5] This shall not be a surprise since factor images are expected to be piece-wise continuous thus form clusters over the joint distribution. It can be further concluded that such joint distribution clusters correspond to the overlapped homogeneous areas of the factor images. Thus, we shall expect to achieve a better factor image decomposition using a subset of pixels that supports the independency of the factor images.

Inspired by such reasoning, we proposed a partially-ICA (PICA) technique in [5]. Rather than using all the pixels that give rise to a large decomposition error due to source dependency, we attempt to (iteratively)

identify a pixel subset supporting source independency and over which to estimate the demixing matrix $\mathbf{W}$ and subsequently factor images $\mathbf{k}(i)$.

Compared with the basic ICA model, where each observation is a linear combination of independent components, our PICA model assumes that each observation x_i is a linear mixture of statistically dependent components $s_1, s_2, ..., s_n$, with an n by n non-singular mixing matrix A, i.e.,

$$\begin{bmatrix} x_1 \\ x_2 \\ \\ x_n \end{bmatrix} = \mathbf{A} \begin{bmatrix} s_1 \\ s_2 \\ \\ s_n \end{bmatrix}, \text{ or } \mathbf{x} = \mathbf{As} \tag{8}$$

where

$$\mathbf{s}= \begin{bmatrix} s_1 \\ s_2 \\ \\ s_n \end{bmatrix} = \begin{bmatrix} s_{11} & s_{12} & \cdots & s_{1m} \\ s_{21} & s_{22} & \cdots & s_{2m} \\ \cdots & \cdots & \cdots & \cdots \\ s_{n1} & s_{n2} & \cdots & s_{nm} \end{bmatrix} = [S_1, S_2, ..., S_m], \mathbf{x} = \begin{bmatrix} x_1 \\ x_2 \\ \\ x_n \end{bmatrix} = \begin{bmatrix} x_{11} & x_{12} & \cdots & x_{1m} \\ x_{21} & x_{22} & \cdots & x_{2m} \\ \cdots & \cdots & \cdots & \cdots \\ x_{n1} & x_{n2} & \cdots & x_{nm} \end{bmatrix} = [X_1, X_2, ..., X_m] \tag{9}$$

and m is the number of pixels in each functional image. Our task is to recover the dependent components from observations by still utilizing ICA.

Let us review the mechanism of independent component analysis on basic ICA model. The components S_i are statistically independent, while based on the Central Limit Theorem; the distribution of a sum (observations) of independent random variables (components) tends toward a Gaussian distribution, under certain conditions. Therefore, the procedure that ICA searches for estimates of the components is to find directions, such that the projections of observations on each direction are distributed with most non-Gaussian distribution. This is the reason that ICA algorithm can help find the (statistically) precise estimate of the components if the components are completely independent (except those two ambiguities of ICA on the scale and order of the components). However, it will mislead direction finding if the components are dependent but ICA algorithm is still superimposed on the observations, which are mixtures of the dependent components. Also, it will give rise to a large separation error since all the pixels are utilized for ICA calculation while the components over all these pixels are statistically dependent.

In order to effectively utilize ICA for this problem, an informative pixel index subspace (corresponding to the independent part of the components) needs to be identified. Then we can perform ICA over this subspace to recover the estimated mixing matrix over the subspace. Imposing this mixing matrix over all the pixel indices, the dependent components are then available to be recovered. The key point is to identify the informative pixel indices, over which the components are statistically independent. The difficulty of this approach is that the independent subspace of the components needs to be identified without any statistical information derived from the components themselves: the components are just what need to be recovered. We only have information derived from observations rather than from components. For simplicity, we consider the dependency of the components rather than that of the observations. It is well know that the statistical dependency/independency of the components s could be measured (visualized) by means of scatter plot with m sample points $S_1, S_2, ..., S_m$ in n dimensional space (each dimension corresponds to a component): they consist of dependent/independent components, which we can perform linear/nonlinear regression curve to estimate the statistical relation between n components.

Clearly, when the number of pixels m is much larger than the number of components n, which is the situation for functional imaging, most probably the sample points are clustered into some clusters. Based on this observation, we divide the dependency of the components into two categories: intrinsic dependency and non-intrinsic dependency. By intrinsic dependency of the components, we mean the dependency caused by the linear and/or nonlinear correlation between components over cluster centers. We refer to non-intrinsic dependency of the components as the dependency over sample points inside each cluster. In other words, the intrinsic dependency corresponds to the global dependency among clusters, while non-intrinsic dependency corresponds to the local

dependency among samples in each cluster. For ICA to work well, we need to remove both intrinsic dependency and non-intrinsic dependency of the components. This can be accomplished by removing the pixels that contribute to intrinsic dependency and non-intrinsic dependency of the components, while retaining the informative pixel indices. Finally, we will apply the ICA onto the subset of pixels for effective recovery of the components over those informative pixel indices.

Notice that both intrinsic dependency and non-intrinsic dependency of the components should be removed with only the information from observations rather than from components. A possible approach to remove intrinsic and non-intrinsic dependencies can be summarized as follows. The intrinsic dependency of the components can be removed by removing all of the clusters except one. The non-intrinsic dependency of the components can be alleviated by removing some sample points in the remained cluster. We will describe the removal procedures next.

3.2.1. Intrinsic dependency removal

In order to remove intrinsic dependency of the components from the observations, the joint distribution of the observations is estimated with Expectation-Maximization (EM) algorithm initialized by k-means method. We assume that the number of clusters t is known with some prior knowledge of the problem. In our DCE-MRI study of breast tumor, the prior knowledge tells us that this number should be two considering the fast-flow and slow-flow characteristics of the breast tumor. Assume that the distribution of the observations is in the following form:

$$p(x) = \sum_{i=1}^{t} \pi_i p(x; m_i, \sigma_i^2) \tag{10}$$

where $p(x; m_i, \sigma_i^2)$ is the ith Gaussian distribution with m_i and σ_i^2 as its mean and variance, and π_i is the weight of the ith Gaussian distribution, $\sum_{i=1}^{t} \pi_i = 1$. Notice that each Gaussian distribution forms a cluster in scatter plot of the observations.

We remove intrinsic dependency of the components in a statistical way. Each sample point X_j is removed in observation scatter plot statistically, with the probability of

$$p_{r1}(\text{removal of } X_j) = \frac{p(X_j) - \pi_k p(X_j; m_k, \sigma_k^2)}{p(X_j)} \tag{11}$$

where k is the index of the remaining cluster.

3.2.2. Non-intrinsic dependency Removal

For removal of non-intrinsic dependency of the components, the remained sample points in scatter plot of the observations are statistically down-sampled with P_θ as its parameter, i.e., X_j is removed statistically with the probability of

$$p_{r2}(\text{removal of } X_j) = \begin{cases} \pi_k p(X_j; m_k, \sigma_k^2) - P_\theta & \text{, if } \pi_k p(X_j; m_k, \sigma_k^2) \geq P_\theta \\ 0 & \text{, otherwise} \end{cases} \tag{12}$$

As a result, the remained sample points in scatter plot of the observations would be uniformly distributed. It is important that the statistical dependency of the components over the corresponding sample points are removed without any destruction of the linear dependency of the observations over the remained sample points. In fact, this dependency should not be removed for the following ICA computation, because the observations over the remained sample points are still the linear mixing of the components, which are statistically independent over the corresponding sample points from the PICA model.

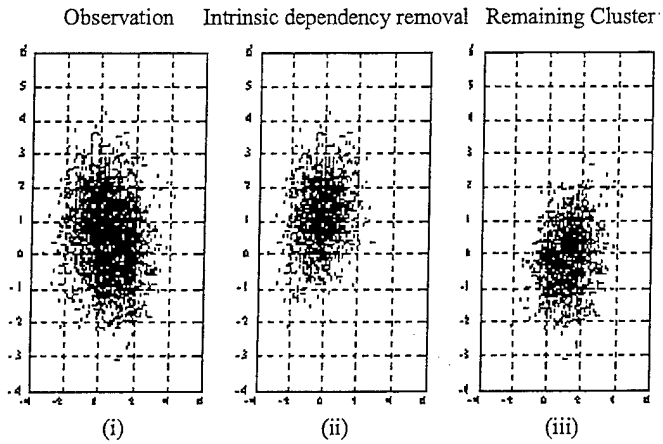

Figure 2. Removal of the intrinsic dependency between the components: (i) observation consists of more than one cluster; (ii) the removal of intrinsic cluster dependency; (iii) the remaining cluster after the removal of intrinsic dependency.

3.2.3. Proposed Algorithm

Assume I is the remained sample point index subset, which is obtained by the removal of intrinsic dependency and non-intrinsic dependency of the components from the scatter plot of the observations. I corresponds to the independent pixel index subspace of the components. We have following procedure for a composite separation of observations:

Step 1: estimate the joint distribution $p(x)$ of the observations with EM algorithm initialized by k-means method, where the number of clusters t is assumed to be known from some prior knowledge;

Step 2: remove intrinsic dependency of the components by a statistical cluster removal method with eq. 11, and remove non-intrinsic dependency of the components by a statistical down-sampling method by utilizing eq. 12 with parameter P_θ, both in the scatter plot of the observations; assume the retained pixel index subset is I;

Step 3: perform ICA on the retained part of the observations, $\{X_j, j \in I\}$, to obtain the estimated mixing matrix A. Since the observations over the retained pixel index subspace I are independent, which satisfies the assumption of basic ICA model; the mixing matrix $\mathbf{A}$ is expected to be better estimated except the ambiguity of scaling and ordering.

Step 4: impose the estimated mixing matrix on the observations over entire indices to obtain the estimated components, i.e., $\mathbf{s} = \mathbf{A}^{-1}\mathbf{x}$.

There are two parameters, t and P_θ, in the above algorithm. t is set with some number by prior knowledge of the problem, while P_θ is a trade-off parameter for controlling the uniformity of the distribution over the sparseness of the sample points in the scatter plot of observations after the removal procedures. The smaller the P_θ is, the more uniform the distribution of sample points over the index subspace looks like, and the less sample points over the index subspace will be. The directions searched out for the sample points over the index subspace with ICA algorithm determine the rows of the estimated mixing matrix. Theoretically speaking, if the parameter P_θ is set smaller, the more uniformed distribution of the sample points in scatter plot of the observations over the index subspace will merit this direction searching; On the other hand, the number of sample points becomes less that limits the sample points to form that distribution, demeriting this direction searching.

4. RESULT AND DISCUSSION

We first applied our method to two computer simulation phantoms for the removal of intrinsic dependency and non-intrinsic dependency among components. Then we applied our method to a data set generated by compartment models, and a real DCE-MRI data set of tumor heterogeneity study.

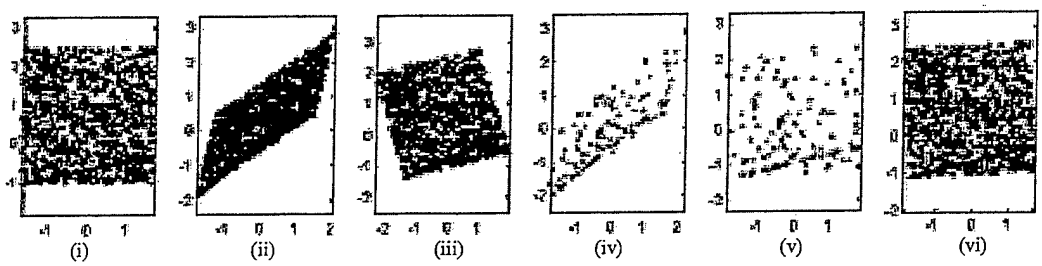

(a) The situation of linear dependency between components

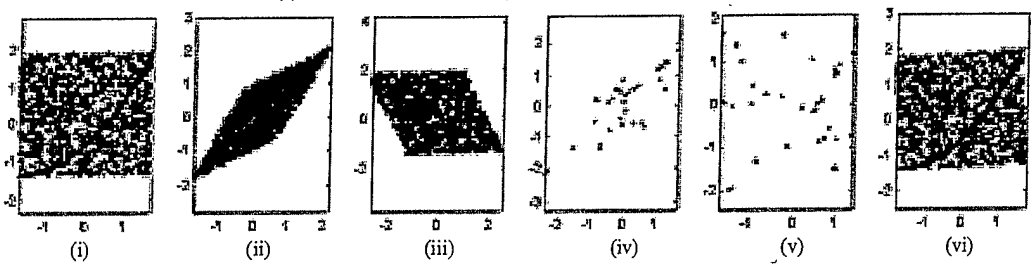

(b) The situation of non-linear dependency between components

Figure 3. The scatter plots of the component recovery process, for both linear (a) and non-linear (b) dependency cases, with ICA and PICA method, (i) components, (ii) observations, (iii) recovered components from ICA method, (iv) observations over the informative index subspace, (v) recovered components over the informative index subspace, (vi) recovered components over full index space from PICA method.

4.1. Phantom study

Figure 2(i) shows the data set that is generated by a sum of two Gaussian distributions: centered at (0,1) and (1,0) with standard variations as two components. Clearly, the components are not independent (i.e., they are intrinsically dependent), and the removal of either Gaussian distribution makes the sample points over the index subspace statistically independent (see Figure 2(ii) and (iii)).

The next data set is generated such that the two components are independent in their first half (left half), and have linear/non-linear correlation for the other half (right half), both with uniformly distributed intensities. The mixing matrix is randomly generated to form observations. Clearly there is a linear/non-linear non-intrinsic dependency between the components in this experiment. Figure 3 (upper/lower figure) shows the scatter plots in the component recovery process with ICA and PICA methods for the situation of linear/non-linear dependency between the components. Figure 4 shows the component recovery process, where the randomized intensities of the first half and the second half are shown in two-dimensional images. Note that the pixels for the first component in the figure are reordered according to its intensities. Evidently, the estimated components recovered by PICA method are much closer to the ground truth of the components by comparing both the scatter plots in Figure 3(i), (iii), (vi) and the images in Figure 4(ii), (iv), (vi).

4.2. Experiments on compartment model

A compartment model is used to simulate the dynamic behavior of the breast tumor obtained with a DCE-MRI sequence. The mask for the fast-flow (FF)/slow-flow (SF) patterns, as well as the overlap region of FF and SF, is shown in Figure 5(a). The pixel intensity in the FF-dominant region/overlap region/SF-dominant region is a linear combination of FF and SF patterns with the corresponding intensity weights of 0.9/0.5/0.1 and 0.1/0.5/0.9. In Figure 5(a), bright/dark gray color corresponds to FF/SF region, and the light gray/dark corresponds to overlap/background, respectively. From the compartment model, we can get a sequence of images shown in Figure 5(b). Our task is to identify the FF and SF patterns hidden in the observed sequence of images.

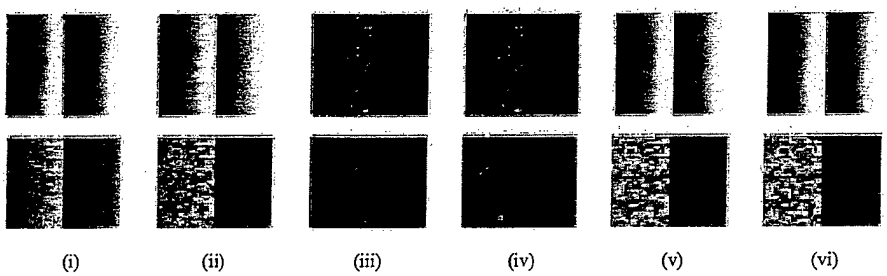

(a) The situation of linear dependency between components

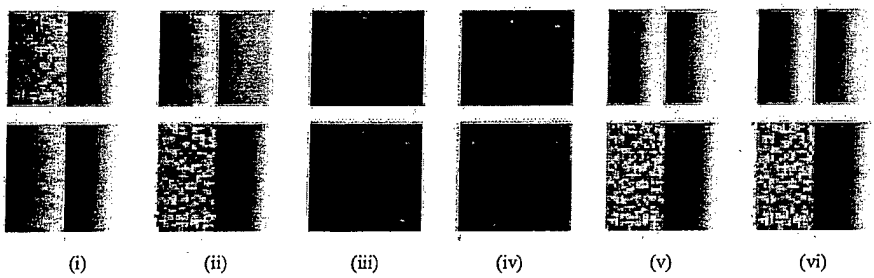

(b) The situation of non-linear dependency between components

Figure 4. Recovery results from ICA and PICA, (i) observations, (ii) recovered components by utilizing ICA method, (iii) observations over the informative index subspace, (iv) recovered components over the informative index subspace, (v) recovered components over full index space by utilizing PICA method, (vi) real components.

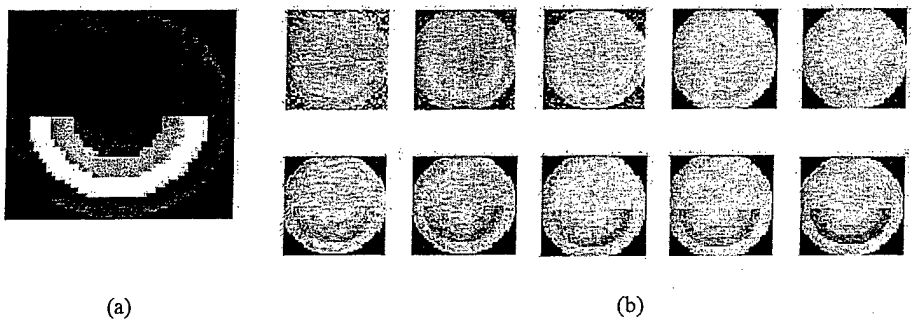

Figure 5. A simulater tumor phantom inclusing fast and slow kinetic subregions; (a) Image mask in compartment model, (b) The sequence of images from the compartment model with the mask shown in (a)

We applied our PICA method to separate the observed composite images into two FF and SF patterns, as well as to have the time-activity curve (TAC). The only two spatial patterns, FF and SF, which is a prior knowledge of this problem, induced us to make an assumption of two components from the observed image sequence. Thus, we divided the image sequence into the first half of the sequence and the second half of the sequence, according to the time index. Then PICA was performed for each pair of observed images, one from the first half, and another from the second half, and the corresponding components were estimated. The final estimation of the components (spatial FF/SF patterns) was attained by averaging all of the estimated components obtained from each pair of observed images. Figure 6 shows the spatial FF/SF pattern and the corresponding TACs achieved by PICA, together with those by ICA for comparison. Notice that each TAC according to the compartment model should be a positive curve. Figure 6(a) shows a better performance for the estimation of the FF and

SF patterns, which are closer to the ground truth of 0.9:0.5:0.1 and 0.1:0.5:0.9/0.9:0.3:0.1 and 0.1:0.7:0.9 from Figure 6(a)(i)/(ii). It is shown from Figure 6(b) that TACs from PICA are better than those from ICA, since they are both approximately positive and more fit to the meaning of dynamic fast-flow and slow-flow activity of the tumor tissue.

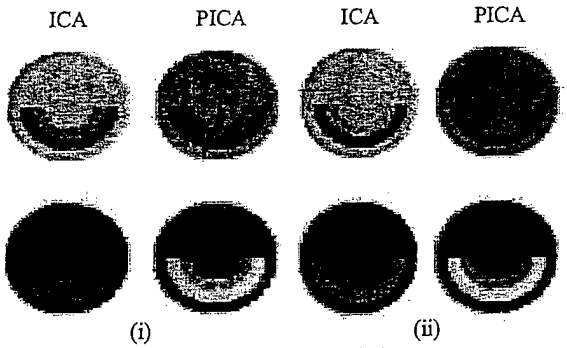

(a) The recovered spatial FF/SF patterns

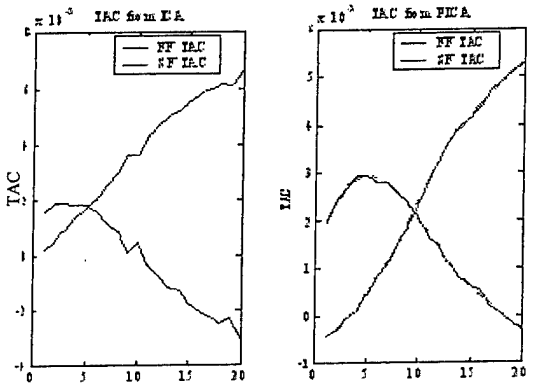

(b) The corresponding TACs

Figure 6. ICA and PICA result, (a) the factor images results for compartment model with FF:overlap:SF region intensity for FF pattern and for SF pattern to be 0.9:0.5:0.1 and 0.1:0.5:0.9/0.9:0.3:0.1 and 0.1:0.7:0.9 respectively; (b) the corrseponding TACs.

4.3. Experiment on real DCE-MRI data set

We tested our PICA method with a real DCE-MRI sequence of breast tumor studies. Figure 7 shows a typical sequence of breast tumor DCE-MRI study. Compared with results from the direct application of ICA, our results using PICA shown in Figure 8, were quite promising in the extracted factors that closely resemble the expected characteristics of compartmental kinetics of tumors. The factor images and the TACs reveal regional distribution of the FF and SF patterns.

ACKNOWLEDGMENTS

This work was supported by the US Army Medical Research and Materiel Command under Grants DAMD17-00-0195 and DAMD17-98-8045.

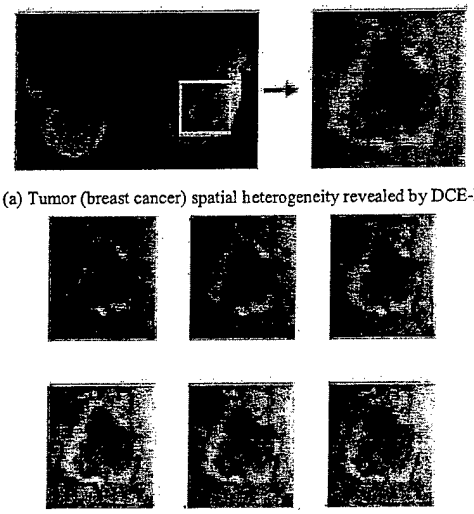

Figure 7. (a) Tumor (breast cancer) spatial heterogeneity revealed by DCE-MRI; (b) Sequences of the breast tumor ROI.

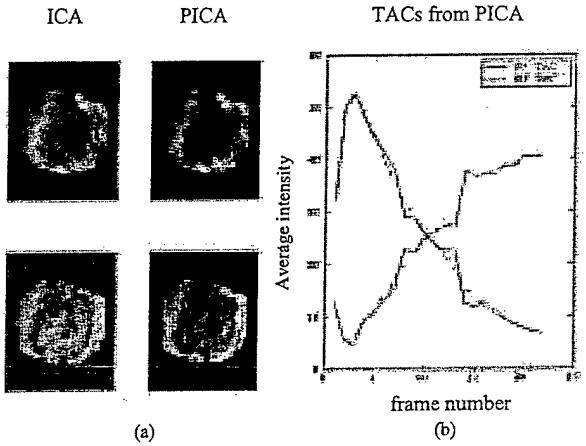

Figure 8. The recovered factor images of the breast cancer spatial heterogeneity and the corresponding TACs revealed by DCE-MRI with PICA method

REFERENCES

1. Z. Szabo, P. F. Kao, W. B. Mathews, H. T. Ravert, J. L. Musachio, "Positron Emission Tomography of 5-HT Reuptake sites in the human brain with C-11 McN5652 Extraction of characteristic images by artificial neural network analysis," *Behavioral Brain Research*, vol.73, pp.221-224, 1996.
2. Y. Zhou, S-C Huang, T. Cloughesy, C. K. Hoh, K. Black, and M. E. Phelps, "A modeling-based factor extraction method for determining spatial heterogeneity of Ga-68 EDTA kinetics in brain tumors," *IEEE Trans. Nuclear Sci.*, vol. 44, no. 6, pp. 2522-2527, Dec. 1997.

3. R. N. Gunn, Steve R. Gunn, and V. J. Cunningham, "Positron emission tomography compartmental models," *J. Cerabral Blood Flow and Metabolism*, vol. 21, no. 6, pp. 635-652, 2001.
4. PKIN: Kinetic Modeling, http://www.pmod.com/doc/PkinReference.html.
5. Y. Wang, J. Zhang, K. Huang, J. Khan, and Z. Szabo, "Independent component imaging of disease signatures," *Proc. IEEE Intl. Symp. Biomed. Imaging*, pp. 178-181, July 7-10, Washington, DC 2002.
6. W. J. Geckle and Z. Szabo, "Physiologic factor analysis (PFA) and parametric imaging of dynamic PET images," *IEEE Symposium on Medical Imaging*, 1992.
7. L. Cinotti, J. P. Bazin, R. DiPaola, H. Susskind, and A. B. Brill, "Processing of Xe-127 regional pulmonary ventilation by factor analysis and compartmental modeling," *IEEE Trans. Med. Imaging*, vol. 10, no. 3, pp. 437-444, 1991.
8. J. Y. Ahn, D. S. Lee, J. S. Lee, S. K. Kim, G. J. Chon, J. S. Yeo, S. A. Shin, J. K. Chung, and M. C. Lee, "Quantification of regional myocardial blood flow using dynamic H215O PET and factor analysis," *J. Nuclear Med.*, vol. 42, no. 5, pp. 782-787, May 2001.
9. H. H. Harman, *Modern Factor Analysis*, University of Chicago Press, 2nd Ed., 1967.
10. M. Samal, H. Surova, M. Karny, et al., "Enhancement of physiological factors in factor analysis of dynamic studies," *Eur J. Nucl. Med.*, 12: 280-283, 1986.
11. H. Attias, "Independent factor analysis," *Neural Computation*, vol. 11, pp. 803-851, 1999.
12. C-H Lau, P-K D. Lun, and D. Feng, "Non-invasive quantification of physiological processes with dynamic PET using blind deconvolution," *Proc. ICASSP*, vol. 3, pp. 1805-1808, Seattle, WA 1998.
13. D. Y. Riabkov and E. V. R. Di Bella, "Estimation of kinetic parameters without input functions: analysis of three methods for multichannel blind identification," *IEEE Trans. Biomed. Eng.*, vol. 49, no. 11, pp. 1318-1327, Nov. 2002.
14. D. Feng, K-P Wong, C-M Wu, and W-C Siu, "A technique for extracting physiological parameters and the required input function simultaneously from PET image measurements: theory and simulation study," *IEEE Trans. Info. Tech. Biomed.*, vol. 1, no. 4, pp. 243-254, Dec. 1997.
15. K-P Wong, D. Feng, S. R. Meikle, and M. J. Fulham, "Simultaneous estimation of physiological parameters and the input function-in vivo PET data," *IEEE Trans. Info. Tech. Biomed.*, vol. 5, no. 1, pp. 67-76, Mar. 2001.
16. M. I. Gurelli and C. L. Nikias, "EVAM: An eigenvector-based algorithm for multichannel blind deconvolution of input colored signals," *IEEE Trans. Signal Processing*, vol. 43, pp. 134-149, Jan, 1995.
17. L. Tong and S. Perreau, "Multichannel blind identification: from sub-space to maximum likelihood methods," *Proc. IEEE*, vol. 86, no. 10, pp. 1951-1968, Oct. 1998.
18. P. Santago and H. D. Gage, "Quantification of MR brain images by mixture density and partial volume modeling," *IEEE Trans. Med. Imaging*, vol. 12, no. 3, pp. 566-573, 1993.
19. P. Santago and H. D. Gage, "Statistical models of partial volume effect," *IEEE Trans. Image Processing*, vol. 4, no. 11, pp. 1531-1540, 1995.
20. P. Tamayo, D. Slonim, J. Mssirov, Q. Zhu, S. Kitareewan, E. Dmitrovsky, E. S. Lander, and T. R. Golub,"Interpreting patterns of gene expression with self-organizing maps: methods and application to hematopoietic differentiation," *Proc. Natl. Acad. Sci.*, vol. 96, pp. 2907-2912, March 1999.
21. D. M. Titterington, A. F. M. Smith, and U. E. Markov, *Statistical analysis of finite mixture distributions.* New York: John Wiley, 1985.
22. Y. Wang, L. Luo, M. T. Freedman, and S-Y Kung, "Probabilistic principal component subspaces: A hierarchical finite mixture model for data visualization," *IEEE Trans. Neural Nets*, Vol. 11, No. 3, pp. 625-636, May 2000.
23. Z. Wang, J. Zhang, J. Lu, R. Lee, S-Y Kung, R. Clarke, and Y. Wang, "Discriminatory mining of gene expression microarray data," *Journal of VLSI Signal Processing System*, 2003. in press
24. W. J. Rugh, *Linear System Theory*, Prentice-Hall, Inc., 1996.
25. Y. Wang, "Independent component analysis-a book review," *IEEE Trans. Med. Imaging*, vol. 21, no. 7, pp. 839-840, July 2002.
26. A. Hyvarinen, J. Karhunen, and E. Oja, *Independent Component Analysis*, New York: John Wiley, 2001.
27. S. Haykin, *Neural Networks: A Comprehensive Foundation*, 2nd ed., Ney Jersey: Prentice-Hall, 1999.
28. B. S. Everitt, *An Introduction to Latent Variable Models*, London: Chapman and Hall, 1984.